Platinum-Decorated Tin Oxide and Niobium-Doped Tin Oxide PEFC Electrocatalysts: Oxygen Reduction Reaction Activity

T. Tsukatsune,[a] Y. Takabatake,[a] Z. Noda,[b] T. Daio,[b] A. Zaitsu,[b] S. M. Lyth,[c,*] A. Hayashi,[b,c,d,*] and K. Sasaki[a,b,c,d,*,z]

[a]*Faculty of Engineering, Department of Hydrogen Energy Systems, Kyushu University, Nishi-ku, Fukuoka 819-0395, Japan*
[b]*International Research Center for Hydrogen Energy, Kyushu University, Nishi-ku, Fukuoka 819-0395, Japan*
[c]*International Institute for Carbon-Neutral Energy Research (WPI-I2CNER), Kyushu University, Nishi-ku, Fukuoka 819-0395, Japan*
[d]*Next-Generation Fuel Cell Research Center (NEXT-FC), Kyushu University, Nishi-ku, Fukuoka 819-0395, Japan*

Using tin oxide (SnO_2) and niobium-doped tin oxide (Nb-SnO_2) as alternative electrocatalyst support materials can effectively solve the issue of carbon corrosion in polymer electrolyte fuel cell (PEFC) cathodes. Here, we systematically explore the effect of support surface area, Pt loading, and Pt nanoparticle size on the electrochemistry of these carbon-free electrocatalysts. Reducing the Pt loading leads to an increase in electrochemical surface area, but the specific activity decreases as previously observed in conventional carbon based electrocatalysts. Removing residual chlorine impurities by replacing the H_2PtCl_6 nanoparticle precursor with $Pt(acac)_2$ increases the specific activity. Niobium-doping of the SnO_2 support also results in an increase in specific activity, due to the increased electronic conductivity. Consequently, the oxygen reduction reaction activity of optimized Pt-decorated Nb-SnO_2 is approaching to that of Pt-decorated carbon black, the current state-of-the-art PEFC electrocatalyst.
 [DOI: 10.1149/2.0431412jes]

Manuscript submitted May 16, 2014; revised manuscript received August 12, 2014. Published August 28, 2014. This was in part Paper 1503 presented at the San Francisco, California, Meeting of the Society, October 27–November 1, 2013.

The polymer electrolyte membrane fuel cell (PEFC) is one of the most promising energy conversion technologies for e.g. residential and automotive applications. Pt nanoparticles supported on carbon black are widely used as electrocatalysts.[1–6] However, carbon corrosion is an issue under high cathode potential, resulting in detachment of Pt catalyst particles from the carbon support, and leading to a decrease in electrochemical surface area (ECSA) and oxygen reduction reaction (ORR) activity over time.[2–6] Due to this problem with carbon, alternative support materials have been investigated. Considerable efforts have been made to develop and analyze alternative carbon-based support materials, including graphitized carbon black,[7–9] carbon nanotubes[10–15] and nanofibers,[14,15] mesoporous carbon,[16,17] and graphene.[15,18–20]

To fundamentally solve this technological issue and improve electrocatalyst durability, alternative *carbon-free* electrocatalyst support materials such as tin oxide (SnO_2)[21–29] and titanium oxide (TiO_x)[30–34] have also been proposed. It has been shown that SnO_2 is a promising alternative platinum support, since it has good electronic conductivity and thermochemical stability under the strongly acidic cathode conditions in a PEFC.[28,35–37]

Remarkable retention of ESCA in Pt-decorated SnO_2 electrocatalysts has been demonstrated compared to Pt-decorated Vulcan carbon black, by severe voltage cycling (up to 60,000 cycles) between 0.9 and 1.3 V versus the reversible hydrogen electrode (V_{RHE}) in electrochemical half-cell durability tests.[28] Recently, the high durability has been confirmed in membrane electrode assemblies (MEAs), during more severe voltage cycling between 1.0 and 1.5 V_{RHE}.[29] These studies have demonstrated the stability of Pt-decorated SnO_2 against the start-stop cycles typical in fuel cell vehicles. However, high ORR activity is also required for PEFC cathode electrocatalyst applications and this has not yet been demonstrated. Relatively low ORR activity has been reported to date compared with state-of-the-art Pt supported on carbon black.[28,36] Most of the ORR values have been measured below 0.9 V_{RHE} for oxide-supported electrocatalysts, while the ORR of conventional Pt-decorated carbon black is usually evaluated at 0.9 V_{RHE}.[2,9,38] Both higher ORR activity and longer durability should be simultaneously fulfilled for practical PEFC applications.

The aim of this study is to obtain sufficiently high ORR activity with high ECSA in Pt-decorated SnO_2-based electrocatalysts by optimizing the preparation protocols. We prepare Pt-decorated SnO_2 (Pt/SnO_2) and niobium-doped SnO_2 (Pt/Nb-SnO_2) electrocatalysts, and systematically explore the effect of Pt loading, Pt nanoparticle size, support surface area, and residual Cl^- ion contamination on the ECSA and ORR activity, through detailed half-cell activity measurements and microstructural characterization. ORR activity values including specific activity and mass activity are reported at 0.9 V_{RHE} for these oxide-supported *carbon-free* electrocatalysts. The guiding factors to improve the ORR activity of PEFC electrocatalysts with SnO_2-based supports are discussed.

Experimental

SnO_2, Nb-SnO_2, and carbon black were used as electrocatalyst support materials in this study. SnO_2 and Nb-SnO_2 were prepared via a precipitation method based on our previous study.[28,29] Diluted NH_3 solution was added to $SnCl_2 \cdot 2H_2O$ ethanol solution at 5°C, followed by filtration and drying in air at 100°C for 15 h. After dry milling, the samples were heat-treated in air at 600°C for 2 h. In the case of Nb-SnO_2, $SnCl_2 \cdot 2H_2O$ ethanol solution and $NbCl_5$ ethanol solution were mixed before co-precipitation, and the final product was $Sn_{0.98}Nb_{0.02}O_2$. For carbon black, commercially available Vulcan XC-72 was used, obtained from Cabot Corp.

Specific surface area and electrical conductivity of these materials were characterized in this study. Specific surface area was evaluated by multipoint Brunauer-Emmet-Teller (BET) analysis based on the nitrogen sorption measurement (BELSORP-mini II, BEL JAPAN, Inc., Japan). For electrical conductivity (σ), their thin layers (area: 0.5 cm^2, thickness: 60 μm) were prepared through the spray printing system (Nordson). Then, their electrical conductivity was determined at 80°C based on the impedance measurements by a four-terminal method (SI 1287, Solartron).

Pt nanoparticles were decorated onto the support materials by two different methods, using two different precursors; chloroplatinic acid (H_2PtCl_6, Kishida Chemical Co., Ltd, Japan),[39] and platinum(II)

*Electrochemical Society Active Member.
zE-mail: sasaki@mech.kyushu-u.ac.jp

Table I. Heat-treatment conditions, ECSA, Pt particle size of electrocatalysts prepared using the H_2PtCl_6 precursor method. Pt loading is 18 wt% in all cases.

Catalysts	Heat-treatment conditions			ECSA [m^2g^{-1}]	Pt particle size [nm]
Pt/SnO_2		100°C		19.8 ± 1.7	4.4 ± 1.3
$Pt/Nb\text{-}SnO_2$	5% H_2 in N_2	100°C	2h	21.4 ± 4.1	N.A.
Pt/Vulcan		200°C		62.7 ± 2.0	N.A.

N.A.: not analyzed.

acetylacetonate ($Pt(acac)_2$, Sigma-Aldrich Co. LLC, USA).[40] In the former method, H_2PtCl_6, $NaHSO_3$, and the support materials were dispersed in distilled water. Then H_2O_2 and NaOH solution were added drop-wise, maintaining pH = 5.0. The dispersion was filtered and the resulting powder dried in air at 100°C for 24 h, then heat-treated at 100°C (for Pt/SnO_2 and $Pt/Nb\text{-}SnO_2$), or at 200 °C (for Pt/Vulcan) in 5% H_2 gas in N_2 for 2 h. In the latter method, $Pt(acac)_2$ dissolved in dichloromethane (Wako Pure Chemical Ind., Ltd., Japan) was added to the support material and stirred in an ultrasonic bath until the solvent was completely evaporated. After dry-milling, the samples were heat-treated in pure N_2. Actual Pt loading was experimentally determined by dissolving Pt in aqua regia. Preparation conditions such as temperature, time, and Pt loading for the electrocatalysts prepared using H_2PtCl_6 and for those using $Pt(acac)_2$ are summarized in Table I and in Table II, respectively. Also, commercially available Pt-decorated carbon black, 46 wt% Pt/C (TEC10E50E, TKK Corp.), was used as a standard catalyst. It was denoted as Pt/C (TKK) in this paper.

The nanostructure was observed using field emission scanning electron microscopy (FESEM, Hitachi High-Technologies Corp., S-5200), scanning transmission electron microscopy (STEM, Hitachi High-Technologies Corp., HD-2200), and high-resolution STEM (JEOL, JSM-ARM200F). Energy dispersive X-ray analysis (EDX, AMETEK Co., Ltd., EDAX Genesis 4000) was applied to analyze the chemical composition.

Half-cell measurements were performed using an automatic polarization system (HZ-5000, Hokuto Denko Corp., Japan) with a 50 mL three-electrode cell (HX-107, Hokuto Denko Corp., Japan). An Au disk electrode (0.196 cm^2) was used as the working electrode, on which the prepared electrocatalyst was carefully deposited. A Pt wire was used as the counter electrode and Ag/AgCl saturated in KCl was used as the reference electrode. Electrocatalyst ink was prepared by ultrasonically dispersing the electrocatalyst powder in ultrapure water, 2-propanol, and 5% Nafion solution. The ink was then deposited onto the Au disk electrode with a loading corresponding to 17.3 μg_{Pt} cm^{-2}. Cyclic voltammetry (CV) measurements were made in a potential range between 0.05 and 1.2 V_{RHE} at a scan rate of 50 mV s^{-1} in N_2-saturated 0.1M $HClO_4$ solution at 25°C. The ECSA of Pt nanoparticles was determined by integrating the area of the hydrogen desorption region (0.05 − 0.4 V_{RHE}) in the CV diagram. ORR activity was characterized by measuring the kinetic current, determined from rotating disk electrode (RDE) measurements. The rotation speed was set at various rates from 2500 to 400 rpm, and the potential was swept from 0.2 to 1.2 V_{RHE} at a scan rate of 10 mV s^{-1} at 25°C, according to the protocols proposed by the Fuel Cell Commercialization Conference of Japan (FCCJ).[41] Specific activity (j_s) and mass activity (j_m) were measured at 0.85 and 0.9 V_{RHE}.

Residual impurity concentration from electrocatalysts was analyzed by dispersing and boiling them in ultrapure water. Then, residual Cl^- ion content was measured by inductively coupled plasma atomic emission spectroscopy (ICP-AES, Agilent Technologies Inc., 7500c), with a detection limit of ca. 0.25 ppm for Cl^- ions, which was experimentally derived from the calibration curve.

Results and Discussion

Characterization of support materials.— Specific surface area of SnO_2, $Nb\text{-}SnO_2$, and Vulcan was 19.3 m^2g^{-1}, 24.7 m^2g^{-1}, and 225 m^2g^{-1}, respectively. Electrical conductivity (σ) of SnO_2, $Nb\text{-}SnO_2$, and Vulcan thin layers (area: 0.5 cm^2, thickness: 60 μm) was 3.46 × 10^{-5} S cm^{-1}, 1.1 × 10^{-4} S cm^{-1}, and 1.02 × 10^{-2} S cm^{-1}, respectively. The hypervalent Nb^{5+} ions act as the electron donor to increase electronic conductivity of SnO_2. SnO_2 and $Nb\text{-}SnO_2$ have much smaller specific surface area and lower conductivity than Vulcan.[28] Even so, an increase in conductivity by Nb-doping has been successfully confirmed.

Electrochemical surface area of electrocatalysts.— For electrocatalysts prepared in this study, Pt particle size and ECSA were evaluated and summarized in Tables I and II. Here, electrocatalysts were prepared in several different conditions. By comparing H_2PtCl_6 and $Pt(acac)_2$ precursor methods, the $Pt(acac)_2$ precursor method leads to smaller Pt particles, revealed by comparing 18 wt% Pt/SnO_2 (4.4 nm) in Table I and 18.4 wt% Pt/SnO_2 (3.3 nm) in Table II. The heat-treatment condition of 210°C for 3 h and 240°C for 3h was initially used, but when it was changed to 240°C for 2h only, Pt particles resulted in slightly smaller as seen in the case of 11.6 wt% $Pt/Nb\text{-}SnO_2$ in Table II. That is probably due to the shorter heating time from total of 6 h to 2h. Then, the heating condition of 240°C for 2h was rather used in the latter part of our study.

Regarding to ECSA, it increases with decreasing Pt loading in both cases of Pt/SnO_2 and $Pt/Nb\text{-}SnO_2$ electrocatalysts. The highest ECSA is 63.4 m^2 g^{-1} for 2.8 wt% Pt/SnO_2, and 66.2 m^2 g^{-1} for 3.7 wt% $Pt/Nb\text{-}SnO_2$ as shown in Table II. These are comparable to 62.7 m^2g^1 for 20 wt% Pt/Vulcan as listed in Table I. The ECSA is shown as a function of Pt particle size in Figure 1. The solid line shows the theoretical ECSA calculated under the hypothesis that all Pt nanoparticles are spherical with a density of 21.5 m^2 g^{-1}. The experimental ECSA decreases as particle size increases, following the same trend with the theoretical values as expected. The difference between the experimental and theoretical values is attributed to a deviation

Table II. Heat-treatment conditions, ECSA, and Pt particle size of electrocatalysts prepared using the $Pt(acac)_2$ precursor method.

Electrocatalyst		Heat-treatment conditions		ECSA [m^2g^{-1}]	Pt particle size [nm]
2.8wt% Pt/SnO_2		210, 240°C	3h + 3h	63.4	2.5 ± 0.5
18.4wt% Pt/SnO_2		210, 240°C	3h + 3h	36.8	3.3 ± 0.6
26.6wt% Pt/SnO_2		210, 240°C	3h + 3h	34.4	N.A.
3.7wt% $Pt/Nb\text{-}SnO_2$	N_2	240°C	2h	66.2 ± 2.0	2.6 ± 0.4
8.3wt% $Pt/Nb\text{-}SnO_2$		240°C	2h	60.9 ± 1.1	N.A.
11.6wt% $Pt/Nb\text{-}SnO_2$		240°C	2h	44.2 ± 2.9	2.7 ± 0.6
11.6wt% $Pt/Nb\text{-}SnO_2$		210, 240°C	3h + 3h	39.1 ± 3.1	3.0 ± 0.7
22.5wt% $Pt/Nb\text{-}SnO_2$		240°C	2h	37.3 ± 3.7	3.3 ± 0.9
38.7wt% $Pt/Nb\text{-}SnO_2$		240°C	2h	12.2	4.6

N.A.: not analyzed.

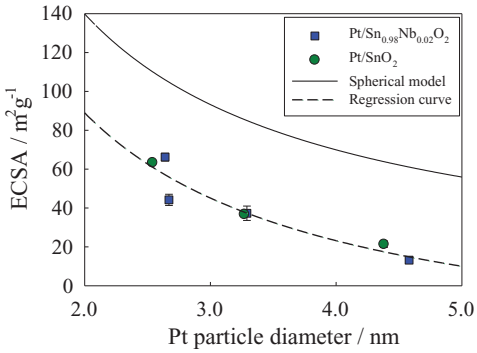

Figure 1. ECSA of Pt/SnO_2 and Pt/Nb-SnO_2 electrocatalysts as a function of Pt nanoparticle size. Theoretical values were calculated using the spherical model (solid line).

from the spherical model, or the presence of an electrochemically inactive interface between the Pt nanoparticles and the oxide support surface.

To understand the interface in more detail, STEM/TEM observation was performed. Figure 2 shows high resolution STEM/TEM micrographs of Pt/SnO_2 with 26.6 and 2.8 wt% Pt loading. The Pt particles are clearly not ideal spheres; approximately half of the Pt surface is bonded to the support. These images indicate that the Pt nanoparticles deviate from the spherical model due to the formation of significant solid-solid interfaces. In the case of the Pt/SnO_2 with higher Pt loading (Fig. 2a), some Pt particles are agglomerated. These deviations from the spherical model account for the overestimate of ECSA in the theoretical calculations. Other factors such as contamination from e.g. the platinum precursor materials may also contribute to the reduced experimental ECSA. This is addressed later in this paper.

The relationship between ECSA and the surface area of supports was also investigated. The support surface area (A_s) is normalized against the supported Pt mass (m_{Pt}) in order to systematically compare the electrocatalysts in this study. Normalized support surface area (A_s/m_{Pt}) is then expressed in Eq. 1, in terms of the BET specific surface area of the support (A_B), and the wt% Pt loading (x_{Pt}):

$$\frac{A_S}{m_{Pt}} = A_B \frac{(100 - x_{Pt})}{x_{Pt}} \quad [1]$$

Using BET specific surface area of the SnO_2 (19.3 $m^2\ g^{-1}$) and Nb-SnO_2 (24.7 $m^2\ g^{-1}$) prepared in this study, the ECSA as a function of A_s/m_{Pt} is plotted in Fig. 3. The ECSA increases with A_s/m_{Pt}, and appears to saturate at high A_s/m_{Pt}. These results indicate that ECSA can increase as long as support surface area is available for the Pt particles to attach to.

STEM micrographs and Pt particle size distributions of 3.7 wt% and 22.5 wt% Pt/Nb-SnO_2 are shown in Figs. 4 and 5, respectively. In the case of Pt/Nb-SnO_2 with 3.7 wt% loading, a homogeneous dispersion of Pt particles with a narrow range in diameters (<4 nm) is observed (Fig. 4). On the other hand, increasing Pt loading to 22.5 wt% (Fig. 5) leads to a broader Pt particle size distribution. This suggests that agglomeration and sintering of Pt nanoparticles in the case of higher loading contributes to lower A_s/m_{Pt} and therefore smaller ECSA. These results show that the low ECSA of Pt/SnO_2 and Pt/Nb-SnO_2 is caused mainly by the low specific surface area of supports. This also explains why the ECSA is comparable to 20 wt% Pt/Vulcan after optimization of the normalized support surface area, A_s/m_{Pt}. An effort to increase specific surface area of supports is therefore necessary for further improvement in the ECSA.

ORR activity.— The specific and mass activities of Pt/Nb-SnO_2, measured at both 0.9 and 0.85 V_{RHE} as a function of ECSA, are shown in Figs. 6 and 7, respectively. Extra data points from our previous study[28,42] and Pt/C (TKK) as the reference are also included to clarify the correlation between ECSA and the specific and mass activities.

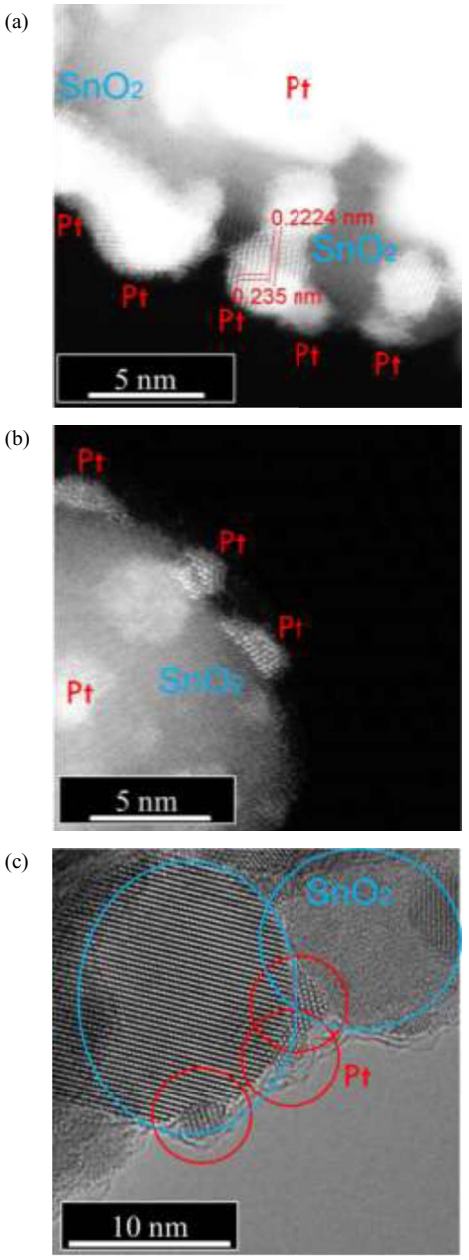

Figure 2. High-resolution STEM images of Pt/SnO_2 with (a) 26.6 wt% loading and (b) 2.8 wt% loading. (c) TEM image of Pt/SnO_2 with 2.8 wt% loading. Pt nanoparticles of a few nm in diameter are dispersed on SnO_2 surface. All samples were prepared using $Pt(acac)_2$.

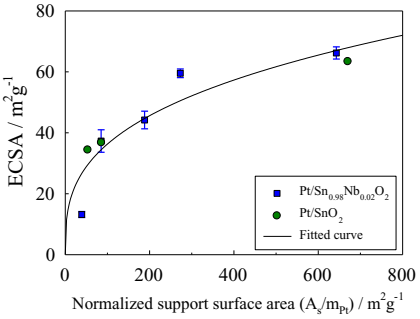

Figure 3. ECSA of Pt/SnO_2 electrocatalysts as a function of the normalized support surface area (A_s/m_{Pt}, i.e. the ratio of the SnO_2 support surface area to the Pt mass).

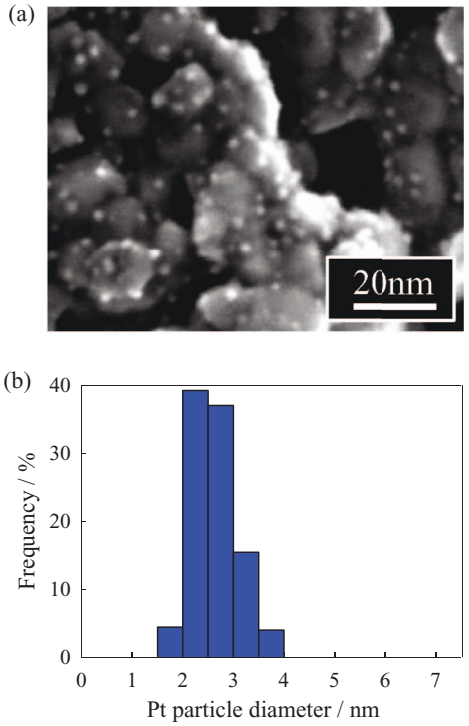

Figure 4. (a) STEM micrograph of 3.7 wt% Pt/Nb-SnO_2 prepared using $Pt(acac)_2$ as a precursor. (b) Pt particle size distribution.

The specific activity tends to decrease with increasing ECSA (Fig. 6). Due to this decrease in specific activity, a high ECSA did not necessarily result in a high mass activity (the product of specific activity and ECSA), as shown in Fig. 7. This may be attributed to the difference in Pt particle size caused by the different wt% Pt loadings. This might lead to an increase in the fraction of oxygen species (such

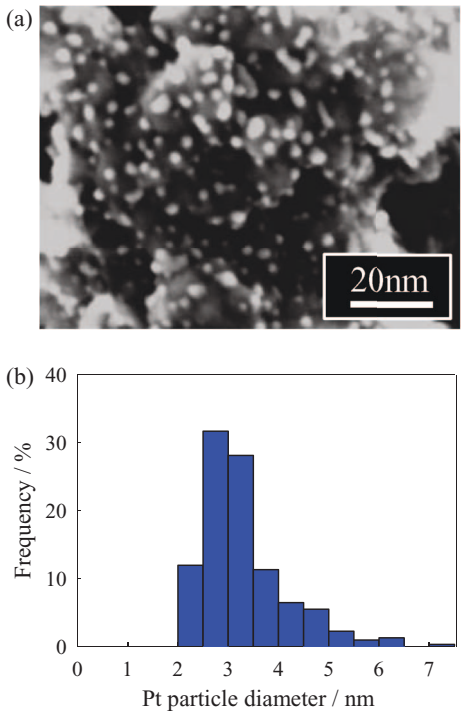

Figure 5. (a) STEM micrograph of 22.5 wt% Pt/Nb-SnO_2 prepared using $Pt(acac)_2$ as a precursor. (b) Pt particle size distribution.

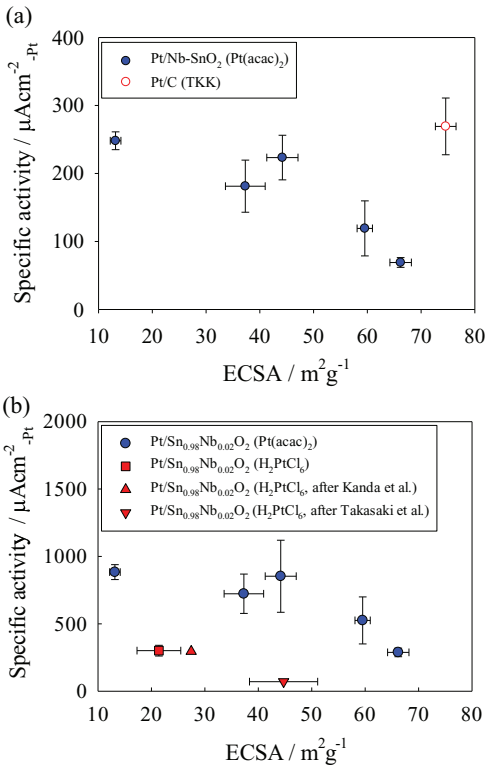

Figure 6. Specific activity at (a) 0.9 V_{RHE} and (b) 0.85 V_{RHE} as a function of ECSA for Pt/Nb-SnO_2 prepared using either $Pt(acac)_2$ or H_2PtCl_6. Extra data points were taken from Kanda et al.[42] and Takabatake et al.[28] Corresponding data for Pt/C (TKK) were also shown as the reference.

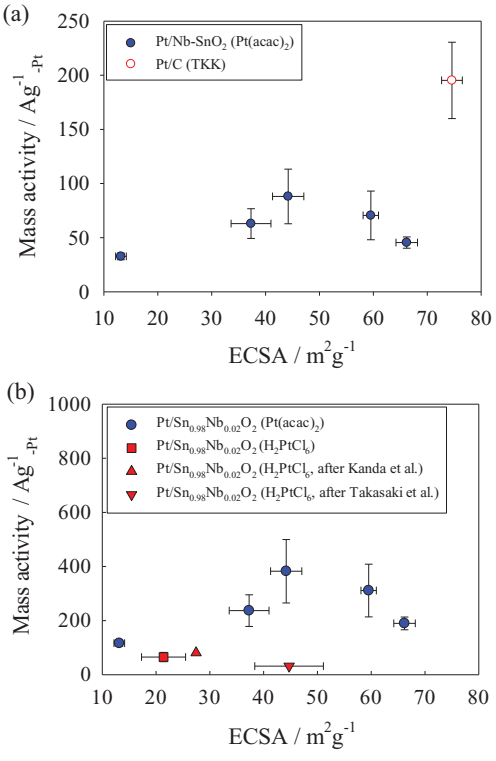

Figure 7. Mass activity at (a) 0.9 V_{RHE} and (b) 0.85 V_{RHE} as a function of ECSA for Pt/Nb-SnO_2 prepared using either $Pt(acac)_2$ or H_2PtCl_6. Extra data points were taken from Kanda et al.[42] and Takabatake et al.[28] Corresponding data for Pt/C (TKK) were also shown as the reference.

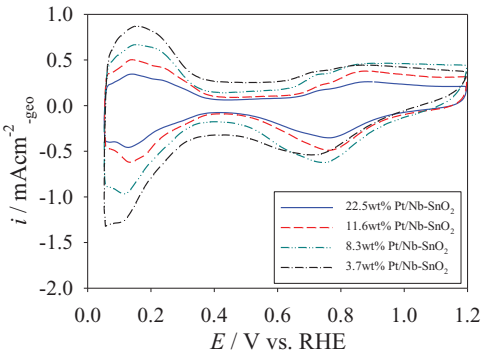

Figure 8. Cyclic voltammograms of Pt/Nb-SnO_2 electrocatalysts with Pt loadings ($Pt(acac)_2$ method).

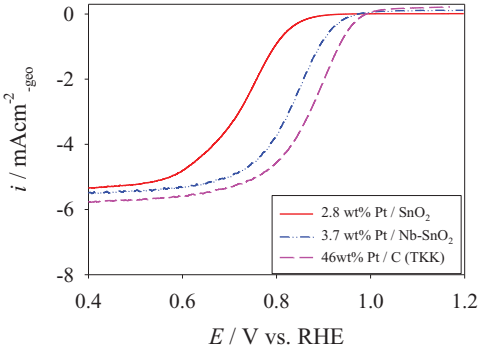

Figure 9. Linear sweep voltammograms for 2.8 wt% Pt/SnO_2 and 3.7 wt% Pt/Nb-SnO_2 prepared from $Pt(acac)_2$, measured using a rotating disk electrode at 1600 rpm. Corresponding data for Pt/C (TKK) were also shown as the reference.

as O_{ad} and OH_{ad}) on the Pt surface at certain potentials, blocking oxygen adsorption sites.[38,43–45] In support of this idea, CV curves of the Pt/Nb-SnO_2 electrocatalysts synthesized from the $Pt(acac)_2$ precursor is shown in Fig. 8. A negative shift in oxygen desorption peak potential is observed at lower Pt loading (3.7 and 8.3 wt%), indicating stronger oxygen adsorption on the Pt surface.[38,45] Consequently, despite lower loading leading to higher ECSA, the specific activity decreases, due to a decrease in Pt particle size. These two opposing tendencies lead to the existence of an optimum condition for mass activity. Alternatively, smaller inter-crystallite distance could also result in a decrease in Pt surface activity.[46]

Additionally, it is clearly shown in Fig. 6 that electrocatalysts prepared using the $Pt(acac)_2$ method have higher specific activity for their ECSA compared to those prepared using H_2PtCl_6 (ca. 20 wt% Pt on SnO_2). This difference could be attributed to residual impurities such as chloride ions (Cl^-). It has been previously shown in the literature that Cl^- ions strongly adsorb onto Pt surfaces and decrease the ORR activity.[43,44] To clarify this effect, Pt/SnO_2 electrocatalysts were prepared using the two different precursors; H_2PtCl_6 and $Pt(acac)_2$. The residual Cl^- ion content was probed by ICP-AES; the catalyst powder was dispersed in ultrapure water and boiled to disperse residual Cl^- ions into solution. Residual Cl^- ions with a concentration of 5.6×10^3 ppm were detected when the H_2PtCl_6 precursor was used, whilst no Cl^- ions were detected using the $Pt(acac)_2$ precursor within the detection limit of the machine. Therefore, we attribute the difference in specific activity to the presence of residual Cl^- ions from the H_2PtCl_6 precursor. Consequently, as expected, residual impurities sensitively affect ORR activity, such that a procedure avoiding Cl^- ions is desired for effective electrocatalyst preparation.

To understand the fundamental electrochemical difference between Pt/SnO_2 and Pt/Nb-SnO_2, linear sweep voltammmograms of 2.8 wt% Pt/SnO_2 and 3.7 wt% Pt/Nb-SnO_2 were evaluated and are shown in Fig. 9 with Pt/C (TKK) as the reference. These two electrocatalysts have similar ECSA and Pt particle size (Table II), such that the effect of particle size on the results (as described above) can be neglected. Simply the effect of Nb-doping can be evaluated. As seen in Fig. 9, Pt/Nb-SnO_2 exhibits higher ORR activity than Pt/SnO_2. ORR activity of Pt/Nb-SnO_2 is approaching to that of Pt/C (TKK). Since donor doping leads to increase in conductivity from 3.46×10^{-5} S cm^{-1} to 1.1×10^{-4} S cm^{-1} as mentioned in the earlier section of this paper, increased electronic conductivity improved the ORR activity. While the heating condition of Pt deposition was slightly different between 2.8 wt% Pt/SnO_2 and 3.7 wt% Pt/Nb-SnO_2, such difference a little influenced on Pt size as explained for 11.6 wt% Pt/Nb-SnO_2 in Table II, and also on ORR. The increase in electrical conductivity was much more effective for ORR.

Even though ECSA of SnO_2 and Nb-SnO_2 can be comparative to Pt/Vulcan or Pt/C (TKK), resulting ORR activity of SnO_2 based electrocatalysts is still lower than carbon based materials owing to their lower conductivity. Whilst hydrogen adsorption/desorption reactions for ECSA measurements may be relatively fast, ORR may be more strongly affected by electron transfer/transport rate-determining by the electrical conductivity of the support materials, leading to a lower ORR activity with SnO_2-based electrocatalyst supports. Other factors affecting ORR activity may not be excluded, such as strong metal-substrate interactions (SMSI), Pt surface defects, and contaminants on Pt catalysts diffused from the support materials.

Conclusions

The electrochemical properties of Pt/SnO_2 and Pt/Nb-SnO_2 were investigated. The dependence of ECSA and ORR activity on Pt particle size, support surface area, Pt loading, and residual Cl^- ion contamination was examined. The ECSA of Pt/SnO_2 and Pt/Nb-SnO_2 electrocatalysts was comparable to Pt/Vulcan after optimization of the normalized support surface area. However, in this study, since the specific surface area of supports was not large enough, an increase in ECSA derived by decreasing Pt particles size resulted in a decrease in specific activity. Therefore, the importance of increasing the specific surface area of oxide support materials for obtaining higher ECSA was shown. Removal of residual Cl^- ions by using an alternative Pt nanoparticle precursor then increased specific activity. Nb-doping of the SnO_2 support also increased the specific activity, due to improved electronic conductivity. Consequently, oxide-supported PEFC electrocatalysts with high ORR activity require oxide supports with; (i) large specific surface area, (ii) high electronic conductivity, and (iii) negligible impurities. These should be the guiding factors when further improving oxide-supported PEFC electrocatalysts in the future.

Acknowledgments

Financial support by the grant-in-Aid for Scientific Research (No. 23226015), JSPS Japan, is gratefully acknowledged. The International Institute for Carbon-Neutral Energy Research is supported by World Premier International Research Center Initiative (WPI), MEXT, Japan. The authors thank S. Matsuie for measuring electrical conductivity of SnO_2-based materials.

References

1. J. Larminie and A. Dicks, *Fuel Cell Systems Explained*, 2nd ed., JohnWiley & Sons, England (2003).
2. W. Vielstich, H. A. Gasteiger, and A. Lamm, *Handbook of fuel cells: fundamentals, technology, and application, fuel cell technology and applications*, Vols. 3 & 4. New York: John Wiley & Sons; 2003.
3. C. A. Reiser, L. Bregoli, T. W. Patterson, J. S. Yi, D. Yang, M. L. Perry, and T. D. Jarvi, *Electrochem. Solid-State Lett.*, **8**, A273 (2005).
4. L. M. Roen, C. H. Paik, and T. D. Jarvi, *Electrochem. Solid-State Lett.*, **7**(1), A19 (2004).
5. J. P. Meyers and R. M. Darling, *J. Electrochem. Soc.*, **153**(8), A1432 (2006).
6. S. Maass, F. Finsterwalder, G. Frank, R. Hartmann, and C. Merten, *J. Power Sources*, **176**, 444 (2008).

7. H. Yano, T. Akiyama, P. Bele, H. Uchida, and M. Watanabe, *Phys. Chem. Chem. Phys.*, **12**, 3806 (2010).
8. M. Hara, M. Lee, C. Liu, B. Chen, Y. Yamashita, M. Uchida, H. Uchida, and M. Watanabe, *Electrochim. Acta*, **70**, 171 (2012).
9. X. Zhao, A. Hayashi, Z. Noda, K. Kimijima, I. Yagi, and K. Sasaki, *Electrochim. Acta*, **97**, 33 (2013).
10. Y. Shao, G. Yin, J. Zhang, and Y. Gao, *Electrochim. Acta*, **51**, 5853 (2006).
11. L. Li and Y. Xing, *J Power Sources*, **178**, 75 (2008).
12. K. Matsumoto, T. Fujigaya, K. Sasaki, and N. Nakashima, *J Mater. Chem.*, **21**, 1187 (2011).
13. D. Sebastián, A. G. Ruíz, I. Suelves, R. Moliner, M. J. Lázaro, V. Baglio, A. Stassi, and A. S. Aricò, *Appl. Catal.*, **B115/116**, 269 (2012).
14. K. Sasaki, K. Shinya, S. Tanaka, Y. Kawasoe, T. Kuroki, K. Takata, H. Kusaba, and Y. Teraoka, *Mater. Res. Soc. Symp. Proc.*, **835**, 241 (2004).
15. C.-L. Lee, C.-H. Huang, K.-L. Huang, Y.-L. Tsai, and C.-C. Yang, *Carbon*, **60**, 392 (2013).
16. P. V. Shanahan, L. Xu, C. Liang, M. Waje, S. Dai, and Y. S. Yan, *J. Power Sources*, **185**, 423 (2008).
17. I. Yagi, A. Hayashi, K. Kimijima, H. Notsu, N. Ohta, and A. Yamaguchi, *Electrochemistry*, **78**(2), 2 (2010).
18. H. Wu, D. Wexler, and H. Liu, *J Solid State Electrochem.*, **15**, 1057 (2011).
19. Y. Li, Y. Li, E. Zhu, T. McLouth, C. Chiu, X. Huang, and Y. Huang, *J Am. Chem. Soc.*, **134**, 12326 (2012).
20. J. Liu, K. Sasaki, and S. M. Lyth, *ECS Trans.*, **58**(1) 1751 (2013).
21. W. S. Baker, J. J. Pietron, M. E. Teliska, P. J. Bouwman, D. E. Ramaker, and K. E. Swider-Lyons, *J. Electrochem. Soc.*, **153**(9), A1702 (2006).
22. T. Takeguchi, Y. Anzai, R. Kikuchi, K. Eguchi, and W. Ueda, *J. Electrochem. Soc.*, **154**(11), B1132 (2007).
23. T. Tada, Y. Yamamoto, K. Matsutani, K. Hayakawa, and T. Namai, *ECS Trans.*, **16**(2), 215 (2008).
24. M. Nakada, A. Ishihara, S. Mitsushima, N. Kamiya, and K. Ota, *Electrochem. Solid-State Lett.*, **10**(1), F1 (2007).
25. K.-S. Lee, I.-S. Park, Y.–H. Cho, D.-S. Jung, N. Jung, H.–Y. Park, and Y.–E. Sung, *J. Catal.*, **258**, 143 (2008).
26. A. Masao, Z. Noda, F. Takasaki, K. Ito, and K. Sasaki, *Electrochem. Solid-State Lett.*, **12** (9), B119 (2009).
27. K. Kakinuma, M. Uchida, T. Kamino, H. Uchida, and M. Watanabe, *Electrochim. Acta*, **56**, 2881 (2011)
28. F. Takasaki, S. Matsuie, Y. Takabatake, Z. Noda, A. Hayashi, Y. Shiratori, K. Ito, and K. Sasaki, *J. Electrochem. Soc.*, **158**(10), B1270 (2011).
29. K. Kanda, Z. Noda, Y. Nagamatsu, T. Higashi, S. Taniguchi, S M. Lyth, A. Hayashi, and K. Sasaki, *ECS Electrochem. Lett.*, **3**(4) F15 (2014).
30. T. Ioroi, Z. Siroma, N. Fujiwara, S. Yamazaki, and K. Yasuda, *Electrochem. Comm.*, **7**, 183 (2005).
31. T. Ioroi, H. Senoh, S. Yamazaki, Z. Siroma, N. Fujiwara, and K. Yasuda, *Electrochem. Comm.*, **7**, 183 (2005).
32. B. L. Garcia, R. Fuentes, and J. W. Weider, *Electrochem. Solid-State Lett.*, **10**(7), B108 (2007).
33. N. Rajalakshmi, N. Lakshmi, and K.S. Dhathathreyan, *Intl. J. Hydrogen Energy*, **33**(24), 7521 (2008).
34. S. Huang, P. Ganesan, and B. N. Popov, *Appl. Catal. B: Environmental*, **96**, 224 (2010).
35. M. Pourbaix, *Atlas of Electrochemical Equilibria in Aqueous Solutions*, 2nd ed., 1974.
36. K. Sasaki, F. Takasaki, Z. Noda, S. Hayashi, Y. Shiratori, and K. Ito, *ECS Trans.*, **33**(1), 473 (2010).
37. Y. Takabatake, Z. Noda, S.M. Lyth, A. Hayashi, and K. Sasaki, *Intl. J. Hydrogen Energy*, **39** (10) 5074 (2014).
38. H.A. Gasteiger, S.S. Kocha, B. Sompalli, and F.T. Wanger, *Applied Catalysis B: Environmental*, **56**, 9 (2005).
39. H. G. Petrow and R. Allen, U.S. Pat. 4,044,193 (1977).
40. A. Hayashi, H. Notsu, K. Kijima, J. Miyamoto, and I. Yagi, *Electrochim. Acta*, **53**(21), 6117 (2008).
41. A. Ohma, K. Shinohara, A. liyama, T. Yoshida, and A. Daimaru., *ECS Trans.*, **41**(1), 775 (2011).
42. K. Kanda, Z. Noda, A. Hayashi, and K. Sasaki, unpublished results.
43. T. J. Schmidt, U. A. Paulus, H. A. Gasteiger, and R. J. Behm., *J. Electroanal. Chem.*, **508**, 41 (2001).
44. V. Stamenkovic, N. M. Markovic, and P. N. Ross Jr., *J. Electroanal. Chem.*, **500**, 44 (2001).
45. K. J. J. Mayrhofer, B. B Blizanac, M. Arenz, V. R. Stamenkovic, P. N. Ross, and N. M. Markovic., *J. Phys. Chem.*, **B109**, 14433(2005).
46. M. Watanabe, H. Sei, and P. Stonehart., *J. Electroanal. Chem.*, **261**, 375 (1989).